Supplement of Atmos. Chem. Phys., 23, 6299–6318, 2023
https://doi.org/10.5194/acp-23-6299-2023-supplement

Atmospheric Chemistry and Physics
Open Access
EGU

Supplement of

The (mis)identification of high-latitude dust events using remote sensing methods in the Yukon, Canada: a sub-daily variability analysis

Rosemary Huck et al.

Correspondence to: Rosemary Huck (rosemary.huck@ouce.ox.ac.uk)

S1. Regional wind context

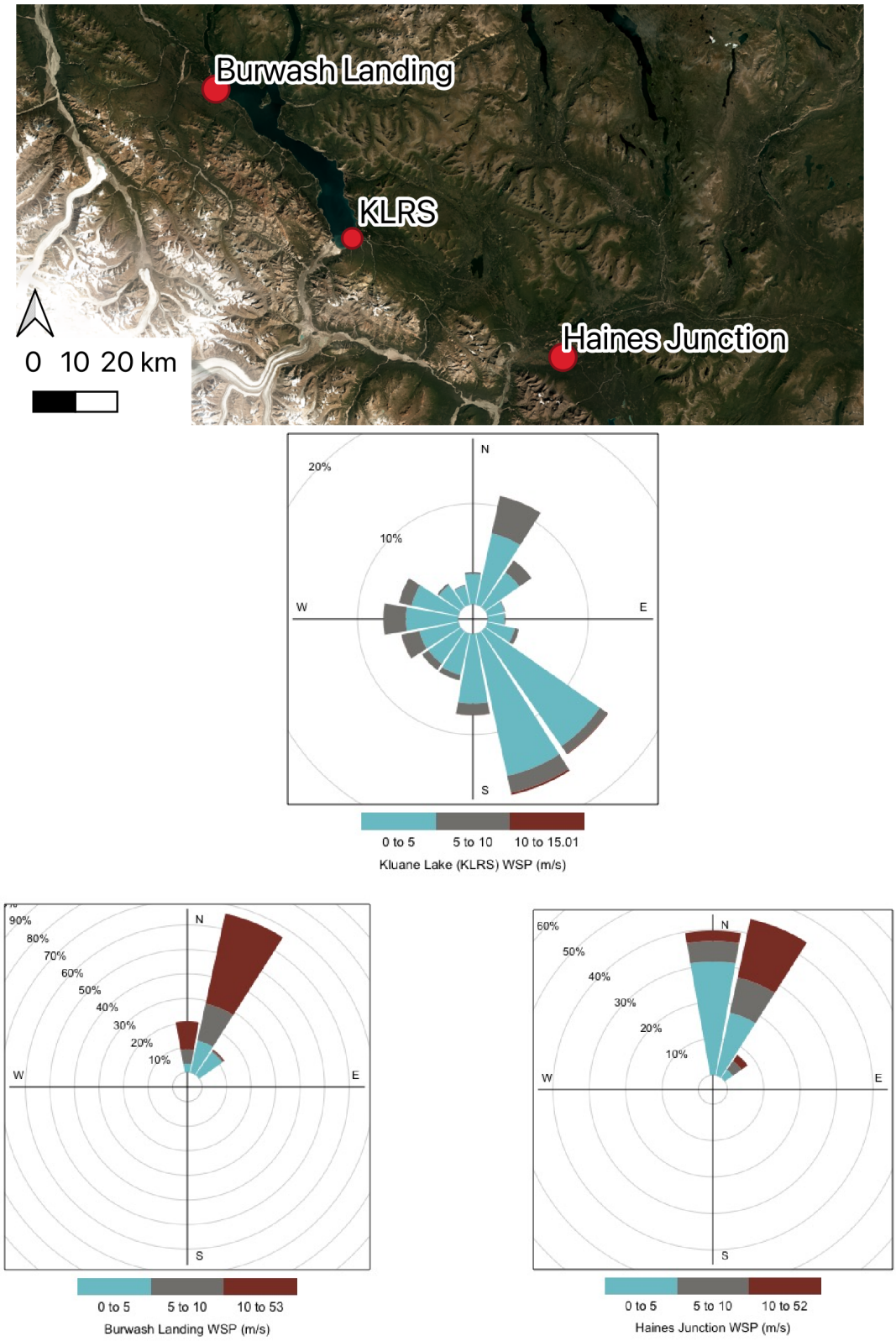

Figure S1. Winds roses from Burwash Landing, Kluane Lake Research Station, and Haines Junction locations for the 2018. Lhù'àän Mân has a much more complex wind regime than the more northerly Burwash Landing and the more southerly Haines Junction stations. Base imagery is from PlanetScope imagery in August 2018.

S2. River diversion at the Kaskawulsh Glacier

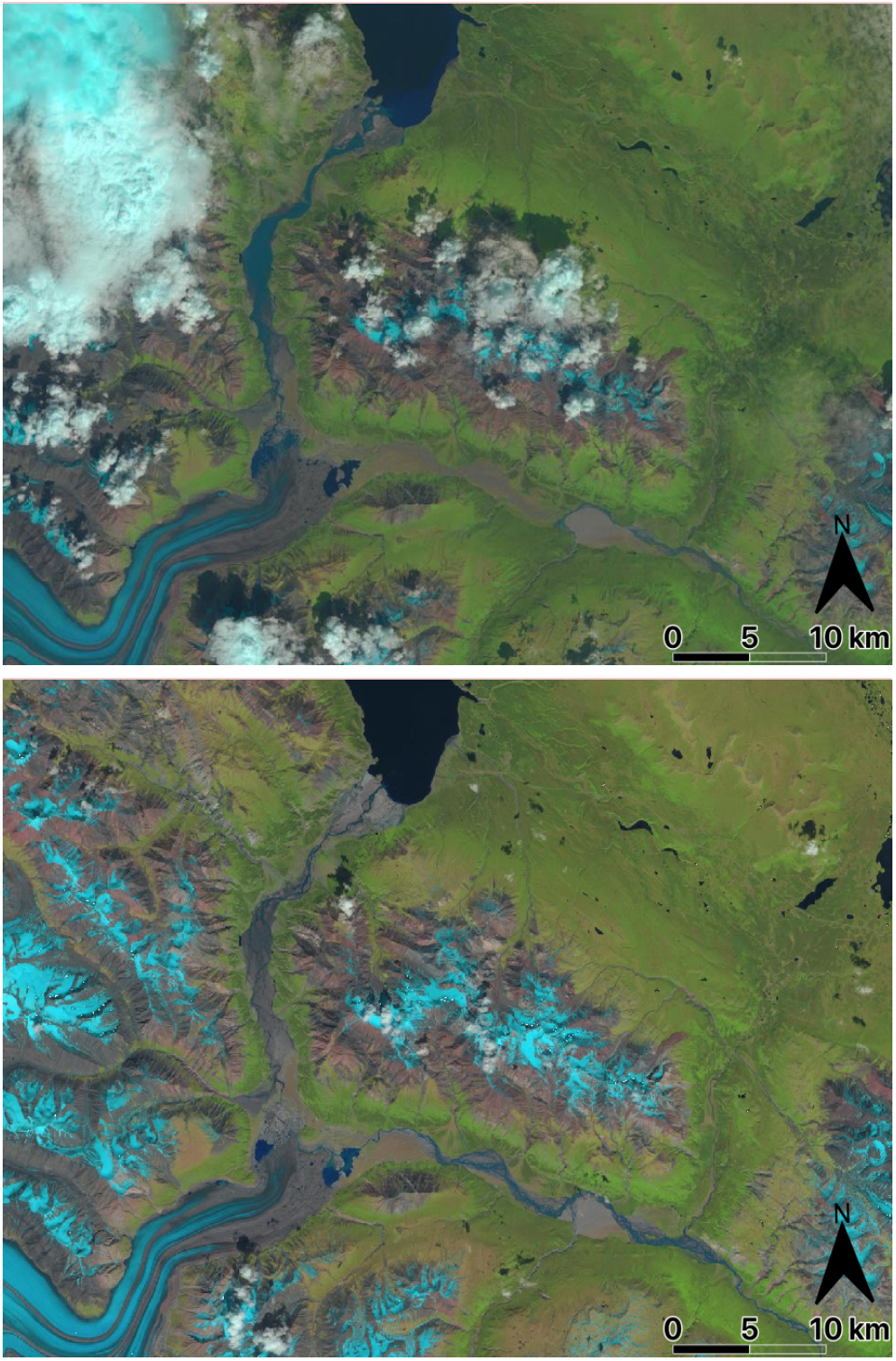

Figure S2. The changes in river flow after glacial retreat and subsequent diversion of the Á'áy Chù to the Kaskawulsh river. True colour Sentinel images show high flow in the northern flowing Á'áy Chù (top image), and low flow in the estuary flowing Kaskawulsh river on 23/06/15. After the sudden draining of the terminus lake in the spring of 2016 increased flow can be seen on the Kaskawulsh river, with reduced flow in the Á'áy Chù (lower image taken on: 14/06/19).

S3. Implications of using Level 1.0 AERONET data

Cloud-screening is an essential part of the AERONET network data refinement. Clouds affect AOD, with cirrus clouds being included in the fine mode AOD and other cloud types having larger optical depths (Arola et al., 2017). To extract errors where the clouds are thin enough to get direct sun measurements, cloud screening is applied to all AEROENT data (Arola et al., 2017). This cloud screening removes around ~20 to 50% of the data (Smirnov et al., 2000), and as seen in figure 9a removes many dust events. To get an accurate image of dust events at the site, level 1.0 data is used, but as a by-product some cloud optical depth may also be included in AOD measurements. Arola *et al*. (2017) found that the uncloud-screened data added roughly 0.007 and 0.0012 onto the AOD. However, these results are proprietary and due to being unable to calculate the effect that cloud screening has at Lhù'ààn Mân and other locations or whether the screened cloud was actually dust, uncloud-screened data was used throughout the study. The SSA and volume size distribution inversion products are run using level 2.0 cloud-screened data. Days recorded as DEDs may have had some of the dust aerosol scans removed by these products and subsequent results.

Table S1. Dust event days and cloudy days at Lhù'ààn Mân over the study period. Cloudy days were decerned by analysing MODIS Terra images and DED decerned using 1020 nm wavelength from Dubovik et al. (2002).

	No. of cloudy days in month	No. of DEDs	No. of coincident DEDs and cloudy days
May-18	24	17	14
Jun-18	23	26	20
Jul-18	21	17	13
Aug-18	24	13	17
Sep-18	17	13	9
Oct-18	24	10	10
May-19	24	19	15
Jun-19	28	20	19
Jul-19	31	17	17
Aug-19	28	20	19
Sep-19	16	15	9
Oct-19	5	1	0

Precipitation is also a good indicator of cloudiness and the size of water droplets in the cloud affect AOD. Figure S4 details monthly rainfall in 2018 at KLRS. Because of the peaks in precipitation and therefore cloudiness, peak months have an increased uncertainty in their AOD.

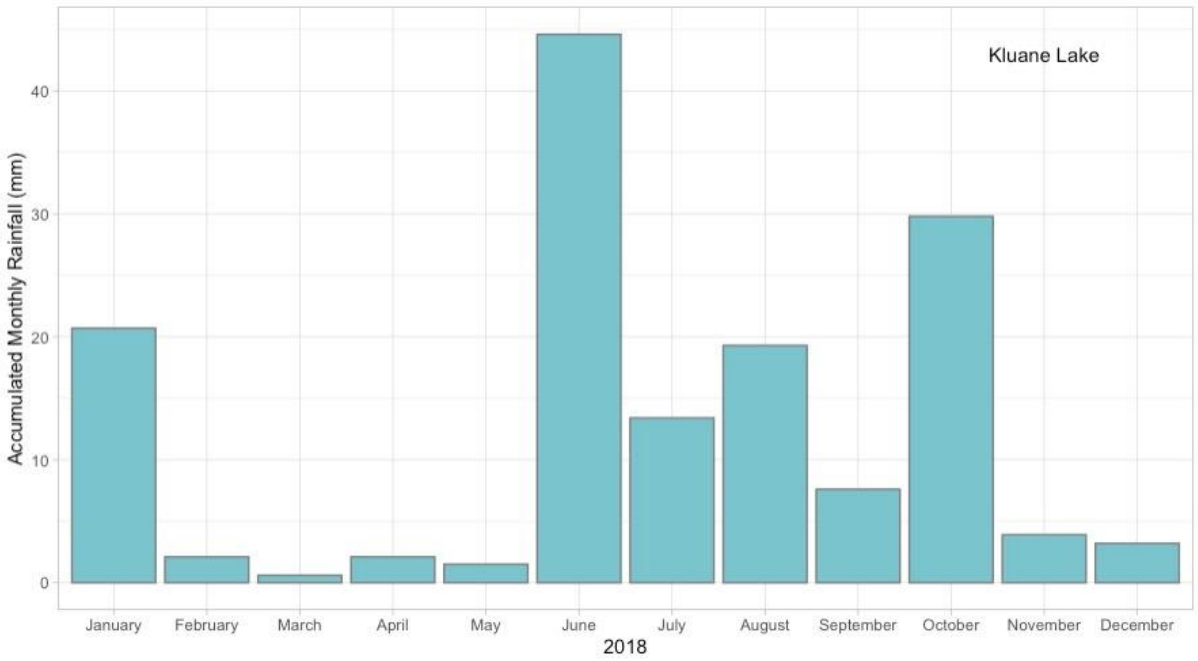

Figure S3. Monthly accumulated rainfall at KLRS in 2018.

S4. Additional information on space-based detection methods

MODIS Terra and Aqua, Sentinel 2 and Landsat 8 true colour images were examined on cloud free days to look for the detection of dust events. Sentinel 2 returned 5 potential dust event days, however due to the lower image resolution of sentinel 2 (10m) it was hard to visually determine if these were dust events or clouds. These images were taken no further in the study as dust plume origin and source geomorphology could not be determined from these images. Landsat 8 has an even lower resolution of 30m and no dust events we detected from Landsat imagery over 2018/19. MODIS Aqua returned 2 potential DEDs and Modis Terra returned 5 potential DEDs (see figure S4), like with Sentinel data it was hard to visually determine if these were dust events or clouds for the majority of events.

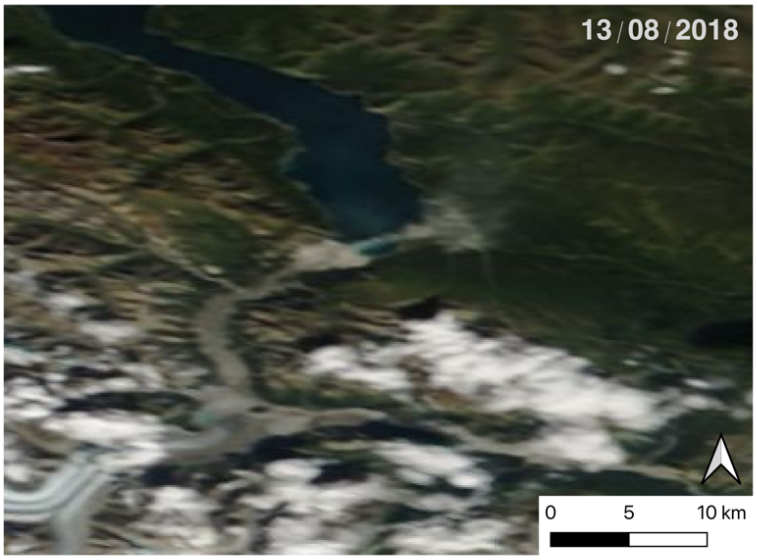

Figure S4. MODIS Terra Image of a dust plume blowing over KLRS on a clear day. Plume length (from end of delta to end of plume) is ~ 8km. (NASA 2018)

S5. MODIS MAIAC and AOD timeline

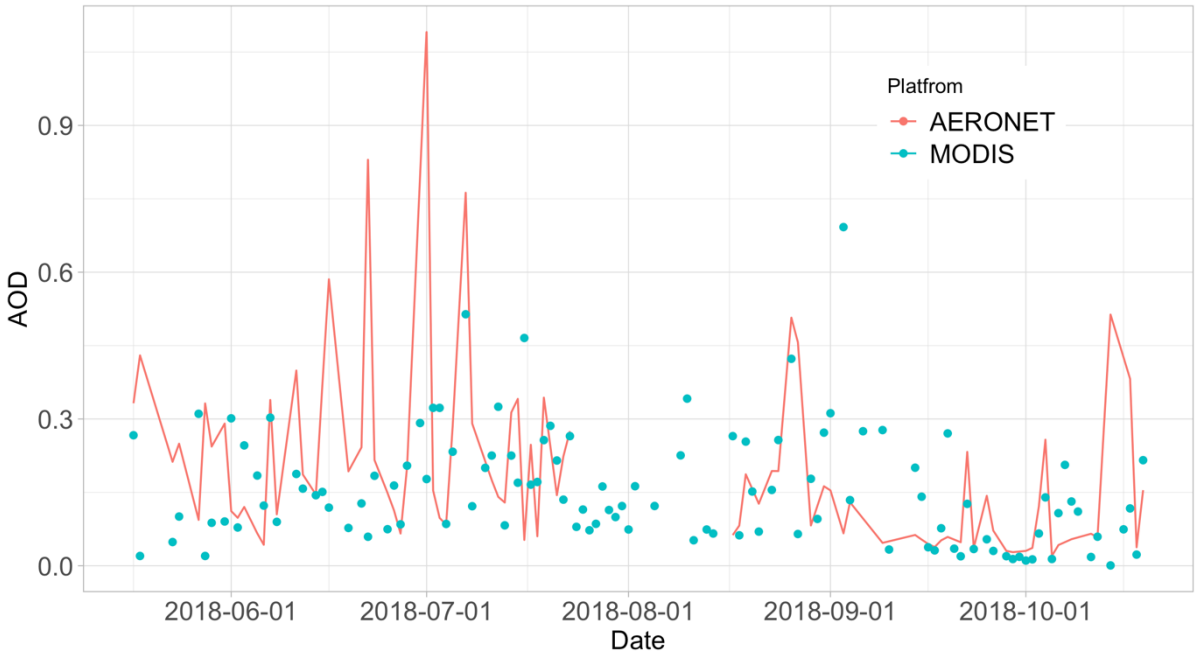

Figure S5. Mean daily MAIAC v6 1km AOD at 470 nm (dashed line) and mean daily AERONET AOD at 500 nm (solid line) returns from 17/05/18 – 17/10/18. Panel A shows the maximum AOD value recorded that day by each platform.

S6. Linking DEDs to sources of dust

The high resolution of PlanetScope imagery (~3 m) provides great insight into the geomorphology of the delta, the detail of which allowed classifying sediment type extending beyond existing geomorphological classifications. If the geomorphology of the delta were mapped following the methods of Bullard et al. (2011) the whole study site would be low relief alluvial which is unarmoured and incised, but the high detail of PlanetScope imagery allows such fine scale sediment differences to be mapped. Figure S4 displays the geomorphology of the Á'áy Chù delta on the 24th May 2018, where multiple types of sediment can be identified. The high-water table is evidenced by the sporadic resurgence of stationary water. The PlanetScope imagery was combined with the oblique camera images to map the origin location of the dust plumes to identify areas where dust is seen to be actively entrained. Identifying dust origins is enhanced by a slight lag of one second between the NIR scan and the RGB PlanetScope scan; when the red and NIR bands are removed, dust is captured in motion at the site. These clear sky-differenced images, alongside the RGB images were then used to locate the origins of the dust plumes in the delta. When the geomorphological map (Figure S4) and dust plume origin map (Figure S4) are combined, the emissive areas and sediment type are established. The highest density of plume origins is located on the southern bank of the river in the medium and light sediment, close to areas of damp sediment. On the northern bank of the river sediment plume origins tend to be close to areas near standing water. Plume origins only occur in the central half of the delta. Strong katabatic winds are topographically channelled down the valley and provide the kinetic energy for MA to be entrained. Before the delta, the valley narrows (Figure S2) channelising the airflow and leaving the area

exposed to the strongest of winds to be spatially restricted around the river, and the majority of dust plumes originate in this area.

Sediment in the Á'áy Chù delta is no longer being replenished by the yearly meltwater flooding of the delta due to the river diversion in 2016. This has dramatically changed the dynamics of MA emission at the site, and surface geomorphology gives a good indication into what surfaces are good emitters. Many of the emissive surfaces identified are located close to damp, dark-toned sediment or standing water bodies. These recently dried out sediments are newly available for entrainment. The recently dried sediment is eroded at a higher rate due to sediment around it that has already been deflated by winds which were unable to entrain the wet sediment. The majority of sediment is entrained from the darkest of surfaces. The darkness of the sediment can be used as a proxy for its moisture content (Mockford et al., 2018). The darker, wetter sediment is constantly being dried out by the wind, making sediment available for entertainment. This supports previous work from the site that confirms that the soil moisture is one of the main controlling factors on MA emission at the site (Nickling, 1978) and emphasises the need for high resolution work to be able predict emissions from the location.

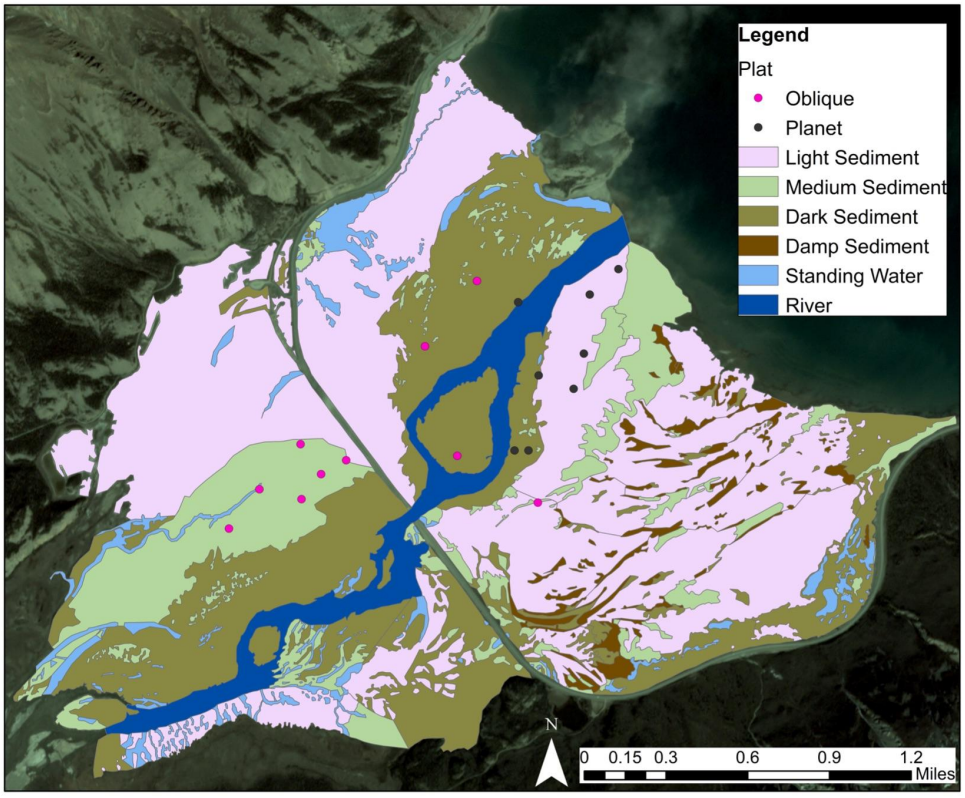

Figure S6. Distribution of different surface conditions on the Á'áy Chù delta on the 24th May 2018 and origins of dust plume on the delta. Geomorphological mapping is based on PlanetScope imagery for the day as well as the oblique camera images. Base imagery is from Planetscope imagery in June 2018.

Bibliography

Arola, A., Eck, T. F., Kokkola, H., Pitkänen, M. R. A., and Romakkaniemi, S.: Assessment of cloud-related fine-mode AOD enhancements based on AERONET SDA product, Atmos. Chem. Phys., 17, 5991–6001, https://doi.org/10.5194/acp-17-5991-2017, 2017.

Bullard, J. E., Harrison, S. P., Baddock, M. C., Drake, N., Gill, T. E., McTainsh, G., and Sun, Y.: Preferential dust sources: A geomorphological classification designed for use in global dust-cycle models, J. Geophys. Res. Earth Surf., 116, https://doi.org/10.1029/2011JF002061, 2011.

Dubovik, O., Holben, B., Eck, T. F., Smirnov, A., Kaufman, Y. J., King, M. D., Tanré, D., and Slutsker, I.: Variability of absorption and optical properties of key aerosol types observed in worldwide locations, J. Atmos. Sci., 59, 590–608, https://doi.org/10.1175/1520-0469(2002)059<0590:voaaop>2.0.co;2, 2002.

Mockford, T., Bullard, J. E., and Thorsteinsson, T.: The dynamic effects of sediment availability on the relationship between wind speed and dust concentration, Earth Surf. Process. Landforms, 43, 2484–2492, https://doi.org/10.1002/esp.4407, 2018.

Nickling, W. G.: Eolian Sediment Transport During Dust Storms: Slims River Valley, Yukon Territory., Can J Earth Sci, 15, 1069–1084, https://doi.org/10.1139/e78-114, 1978.